JAAS

RSC Publishing

PAPER

The effect of the sampling cone position and diameter on the gas flow dynamics in an ICP

Cite this: *J. Anal. At. Spectrom.*, 2013, **28**, 1485

Maryam Aghaei, Helmut Lindner and Annemie Bogaerts

An inductively coupled plasma, connected to a sampling cone of a mass spectrometer, is computationally investigated. The effects of the sampler orifice diameter (ranging from 1 to 2 mm) and distance of the sampler cone from the load coil (ranging from 7 to 17 mm) are studied. An increase in sampler orifice diameter leads to a higher central plasma temperature at the place of the sampler, as well as more efficient gas transfer through the sampler, by reducing the interaction of the plasma gas with the sampling cone. However, the flow velocity at the sampler position is found to be independent of the sampler orifice diameter. Moreover, by changing the sampler orifice diameter, we can control whether only the central gas or also the auxiliary gas can exit through the sampler. Finally, with the increasing distance of the sampler from the load coil, the plasma temperature at the place of the sampler decreases slightly, which might also have consequences for the ion generation and transport through the sampling cone.

Received 28th March 2013
Accepted 25th June 2013

DOI: 10.1039/c3ja50107h

www.rsc.org/jaas

1 Introduction

The inductively coupled plasma (ICP) is the most popular ion source in analytical chemistry for elemental mass spectrometry (MS). The ions are sampled from the plasma by the insertion of a sampling cone into the plasma. As this (metal) sampling cone is relatively cool compared to the plasma temperature, it results in changes in the composition of the plasma gases that come in contact with the metal surface. Indeed, a boundary layer of cooler gases is formed along the surface of the metal. A detailed discussion about the boundary layer between the plasma stream and the sampler orifice, as well as sample introduction, ionization and ion extraction in ICP-MS was presented in 1981 by Houk *et al.*[1] Later on, several studies were performed to investigate the influence of a MS sampler, both upstream and downstream from the interface cone.[2–15] In ref. 2–10, the upstream region, *i.e.*, the plasma, was investigated, but no comparison was made with and without the sampling interface. Measurements in ref. 11–15 were focused on the region downstream from the interface, but did not give information on changes in the plasma itself. A detailed comparison of the plasma characteristics with and without the sampling interface was made experimentally by Houk and coworkers,[16,17] Farnsworth and coworkers[18] and Hieftje and coworkers.[19]

Besides experimental studies, computational investigations also tried to provide a better insight into the ICP when it is coupled with a MS.[20–22] Douglas and French[20] presented an approximate model of the ideal gas flow through the sampling cone which is the so-called hemispherical-sink model. Spencer *et al.*[21,22] applied a Direct Simulation Monte Carlo (DSMC) algorithm to simulate the flow of neutral argon gas through the first vacuum stage of the ICP-MS. Their calculations yielded plasma velocity data in the region a few millimeters upstream from the sampler which were in reasonable agreement with those from experiments. However, the upstream density and plasma temperature gradients were not included and there was no plasma assumed in the model.[21] Lindner and Bogaerts[23] developed a model of an atmospheric pressure ICP which allows rather easy extension to a variable number of species and ionization degrees. In this model for the first time, the gas flow was traced from the injector inlets, and the plasma characteristics were calculated inside the entire ICP torch. An increase of the analytical performance of the ICP by helium addition to the injector gas was reported and a validation of the model by experiments is provided in ref. 24. Later on, a mass spectrometer interface was coupled to this model to investigate the effect of the presence of a sampler on the fundamental plasma characteristics in ICP-MS.[25] In this paper, specifically the coil region of the plasma as well as the region very close to the sampler were studied. These regions are not very experimentally accessible, and thus, not many investigations onthese regions are reported. It should be noted that Winge *et al.* performed a high speed photography study of ICP-MS and showed an off-axis droplet cloud being deflected as it passes into the sampling hole, which supports the pathline profiles we provided in ref. 25 comparing the ICP with and without the sampling cone.

In order to optimize the analytical performance of ICP-MS, a large number of investigations were performed to study the effect of ICP operating conditions on the plasma characteristics.[24–34]

Research group PLASMANT, Department of Chemistry, University of Antwerp, Universiteitsplein 1, B-2610 Wilrijk-Antwerp, Belgium. E-mail: Maryam.aghaei@ua.ac.be

However, only a few studies have focused on the effect of operating conditions on the upstream plasma.[26,33–35] Effects of the rf power, nebulizer flow rate, sample composition and torch-shield configuration on the ion-transport efficiency through the ICP-MS interface have been studied by Macedone *et al.*[26] Gamez *et al.* found that the perturbation in radial distribution of the electron density and the drop in plasma temperature due to the MS interface change with the applied rf power, central gas flow rate and sampling position.[33,34]

We recently investigated the effect of the operating conditions, *i.e.*, central gas and auxiliary gas flow rates, the pressure downstream from the sampler and the forward power, on the upstream plasma characteristics of the ICP in contact with a MS interface.[36] The calculation results were compared with measured data from ref. 26, 33 and 34. An optimum range of injector gas flow rates is dependent on the injector diameter as is indicated in ref. 24. For the used setup with an injector diameter of 1.5 mm, the optimum range of injector gas flow rates is from 1.0 up to 1.4 L min^{-1}, which guarantees the presence and also a proper length of the central channel in the torch. In ref. 34, Gamez *et al.* also demonstrated experimentally that the central channel becomes well-defined only at flow rates above 1.0 L min^{-1}, and in ref. 26 Macedone *et al.* reported the transport efficiency of the aerosol drops at flow rates above 1.4 L min^{-1}. Furthermore, our calculated data showed that the external power of up to 1250 W (for the specific geometry we used) is optimum and Farnsworth's group also reported in ref. 26 that only a power rise of up to 1300 W causes a better transport efficiency while for power values above 1300 W, the transport efficiency decreases, which was in agreement with our computational results. Moreover, it showed that for any specific purpose, it is possible to control whether only the central gas flow passes through the sampler orifice or it is accompanied by the auxiliary gas flow.[36]

Besides the optimization of operating parameters, the effect of geometrical parameters has also been of considerable interest. In 1983 Gray and Date[37] reported that larger sampler orifice diameters than those for boundary layer sampling (*i.e.*, 50–80 μm diameter range) were needed for sampling the bulk plasma (at least 0.2 mm diameter). However, with these larger orifice diameters another problem arose, *i.e.*, a secondary discharge between the plasma and the sampling cone developed, as had also been already explained by Houk *et al.* in ref. 1. The formation of this discharge is also discussed in ref. 17 and 38. Lichte *et al.*,[39] however, reported that due to deposition of material, the sampling orifice becomes smaller and the metal-to-metal oxide ion ratios change. Crain *et al.*[40] reported that matrix effects are affected by the ratio of sampler and skimmer orifice diameters. Vaughan and Horlick[41] also varied the sampler and skimmer orifice diameters, and indicated that the sampler orifice diameter has a major impact on the signal characteristics. Indeed, for oxide forming elements, the MO^+/M^+ signal ratio appeared to be highly dependent on the orifice diameter. This was also reported by Longerich *et al.*[42] In addition, variation in the sampling orifice diameter changes the shape of the signal *versus* the nebulizer flow rate.[41,42] Furthermore, Vaughan and Horlick also indicated that the sampling orifice is the primary location for oxide formation in ICP-MS. However, the range of sampler orifice diameters used in their study was from 0.51 to 0.94 mm, which is smaller than the range used in more recent designs (*i.e.* larger than 1 mm). They also investigated the effect of the skimmer orifice diameter on the analyte signals and reported that this effect is not as dramatic as the effect of the sampler orifice diameter. In the range of small orifices *i.e.* below 1 mm and using LAM-ICP-MS, Günter *et al.* also reported that by decreasing the sampler cone orifice size (0.7 to 0.5 mm), many background intensities can be reduced by up to two orders of magnitude, while maintaining comparable sensitivity.[43] Finally, Taylor and Farnsworth recently investigated the effect of skimmer cone design (for five commercially available skimmer designs) on the shock formation and ion transmission efficiency at the vacuum interface of an ICP-MS.[44] They reported that the strongest shock was recorded for a skimmer with a cylindrical throat, and the weakest shock was produced by a skimmer with the largest diameter and a conical throat. The transmission efficiency increased with the increasing skimmer orifice diameter.

These observations all suggest that the use of interfaces with different orifice sizes can cause a change in the plasma characteristics. In addition to the effect of sampler and skimmer orifice diameters, the place of the sampler itself was also investigated experimentally. Gamez *et al.* studied the effect of sampling position on the plasma characteristics of an ICP[34] and reported that as the MS interface is brought closer to the ICP load coil, the upstream plasma temperature dropped. Finally, Macedone *et al.* also showed that the barium ion number density in the plasma upstream from the sampler drops as the sampling position is reduced.[35]

In the present paper, we investigate the effect of the sampler distance and sampler orifice diameter on the upstream plasma characteristics of the ICP by means of computer simulations to obtain a deeper insight into the effect of these geometrical parameters. Different sampler distances from the load coil and different sampler orifice diameters are considered in the model. Note that another geometrical parameter, *i.e.*, the injector inlet diameter, has already been investigated in ref. 24, so it is kept constant here. The plasma temperature, gas density, electron density and velocity profiles and the path lines of the gas flow inside the coil region as well as in the region close to the MS interface are studied. The calculation results will be compared with measured data from ref. 33 and 34.

2 Description of the model

A commercial computational fluid dynamics (CFD) program, called Fluent v13.0.0 (ANSYS), was used for the calculations.[45] The solver algorithm of the simulation is the so-called coupled algorithm.[45] For defining the heat capacity and thermal conductivity, a number of self-written modules were added as user-defined functions (UDFs), as described in ref. 23. The electric fields were solved as user defined scalars (UDSs) in Fluent. The 2D axisymmetric geometry of the setup is displayed in Fig. 1. The figure of the torch is in scale; however, the whole calculation region is not shown. Indeed, the calculation region

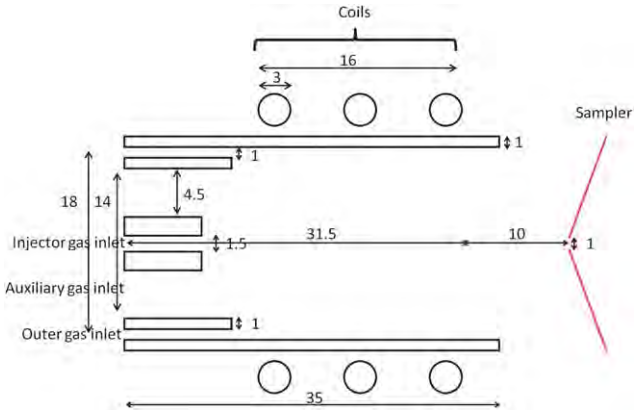

Fig. 1 Schematic picture of the ICP geometry used in the simulation. The data (distances) are given in mm.

has an axial length of 15 cm and a radius of 10 cm. The electric field was assumed to be zero at the border of the calculation region. This can be regarded as the equivalent of the metal shielding box around the ICP, which prevents the rf radiation from entering the laboratory. In our former studies,[25,36] a MS interface (sampler cone) was placed at a distance of 41.5 mm from the gas inlets (10 mm distance from the load coil), on the central axis, and it had a central orifice of 1 mm diameter. In the present work, we performed calculations for different sampler distances from the load coil, ranging from 7 mm to 17 mm. For each sampler distance, we considered three different orifice diameters, *i.e.*, 1 mm, 1.5 mm and 2 mm. In Fig. 1, only the sampler distance of 10 mm with 1 mm orifice diameter is shown.

The gas coming from the three concentric tubes of the ICP torch flows into the sampler cone and towards the open sides of the torch, which are filled with ambient gas, taken to be argon for simplicity. The downstream pressure of the sampler is fixed at 1 torr (1.32×10^{-3} atm) similarly to the experimental setup in ref. 18 and 26. The ambient gas pressure and exhaust pressure are set to 1 atm and 0.99 atm, respectively. The ICP gas stream is assumed to be argon. The plasma species considered in the model are Ar atoms, singly charged and doubly charged Ar ions, and electrons. Their transport properties are calculated by kinetic theory, as is fully described in ref. 23. As discussed in ref. 23 and verified by comparing the calculation results with those from experiments in ref. 24, applying the local thermodynamic equilibrium (LTE) condition to the plasma is a reasonable approximation.

Table 1 Operating and boundary conditions

Frequency	27 MHz
Input power	1000 W
Central gas flow rate	Ar; 1.0 L min^{-1}
Intermediate gas flow rate	Ar; 0.4 L min^{-1}
Outer gas flow rate	Ar; 12 L min^{-1}
Ambient pressure	101 325 Pa
Exhaust pressure	101 225 Pa
Pressure downstream from the sampler cone	1.32×10^{-3} atm (1 torr)
Injector diameter	1.5 mm
Inlet gas temperature	297 K
Sampler cone temperature	500 K
Sampler orifice diameter	1–2 mm
Sampler distance from the load coil	7–17 mm

The gas flow inside the torch is calculated by solving the Navier–Stokes equations. Since the Reynolds number of the flow, even that of the sampler (= 120), is far from the turbulence regime, the laminar flow assumption can be utilized.[45] The model was validated according to the experimental work in ref. 24, 25 and 36. The total power coupled to the plasma is set to 1000 W and the frequency of the harmonic external electric current density is 27 MHz. The plasma, auxiliary and injector gas flow rates are kept fixed at 12, 0.4 and 1.0 L min^{-1}, respectively. The boundary conditions as well as the operating parameters are also displayed in Table 1.

3 Results and discussion

(a) Plasma temperature and gas flow path lines

The temperature and velocity are a result of solving coupled differential equations such as the Navier–Stokes equations and the energy equation, where certain terms are added, *e.g.* power coupling as a source term and the emitted radiation as an energy loss term. The values are calculated by a finite-volume method taking into account the whole calculation region and its boundary conditions. The values are iteratively calculated until a stable solution is found. Fig. 2 shows the 2D plasma temperature distribution (upper frames) and velocity path lines (lower frames) for two different sampler orifice diameters, *i.e.*, 1 mm (left column) and 2 mm (right column), at different sampler positions, *i.e.*, 7 mm (first row), 10 mm (second row) and 13 mm (third row) from the load coil. We performed calculations for a sampling position of up to 17 mm distance from the load coil, but as the pattern is the same in all cases, only the data for a sampling position of 7 mm, 10 mm and 13 mm are shown here for clarity. When comparing the two columns in Fig. 2, it is clear that the outgoing pattern of the auxiliary gas (see black path lines) is quite different when the sampler orifice diameter is changed. At 1 mm diameter, all the auxiliary gas exits through the open sides of the torch, while at 2 mm diameter, the auxiliary gas exits through the sampler orifice and goes to the MS, together with the injector gas.

As demonstrated in ref. 36, the flow pattern of the auxiliary gas can also be controlled by varying the ratio of auxiliary and injector gas flow rates. The results presented in ref. 36 were obtained for an injector diameter of 1.5 mm and a sampler orifice diameter of 1 mm, like in the left column of Fig. 2, but it is clear that changes in the geometrical parameters affect this behavior. Indeed, in the present paper, the injector gas flow rate is higher than the auxiliary gas flow rate (*i.e.*, 1.0 *vs.* 0.4 L min^{-1}; *cf.* above), so according to ref. 36 we would expect to have only the injector gas flowing through the sampler orifice and the auxiliary gas exiting through the open sides of the torch. However, this appears not to be the case for the orifice diameter of 2 mm (see Fig. 2, right column). Indeed, also the ratio between the injector inlet and the sampler orifice diameters plays a role. In the left column, the injector inlet diameter (kept

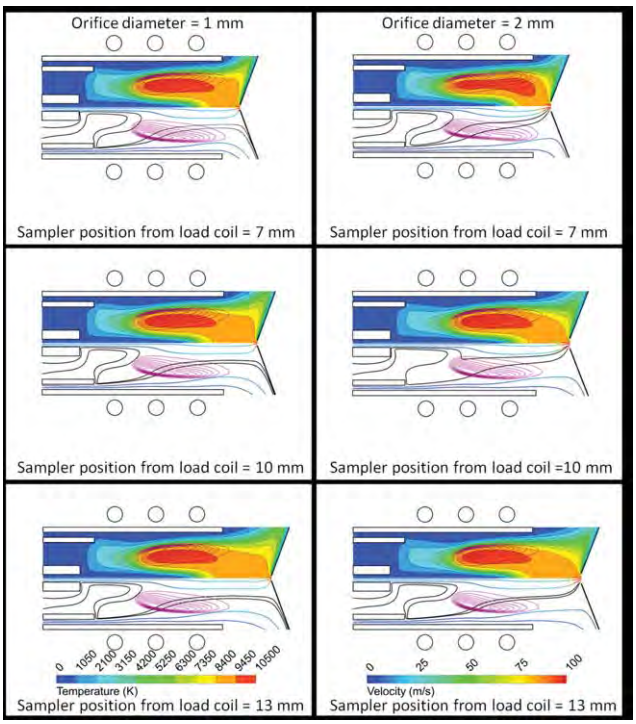

Fig. 2 2D plasma temperature profiles (upper frames) and velocity path lines (lower frames) for 1 mm (left column) and 2 mm (right column) orifice diameter, at a sampler position of 7 mm (first row), 10 mm (second row) and 13 mm (third row) from the load coil. Path lines originating from the injector and outer gas inlets are colored with velocity in m s^{-1}, whereas the path lines from the auxiliary gas are colored in black, to clearly distinguish between the different inlet gases. The red contours demonstrate the area of external power coupling. The injector gas, auxiliary gas and outer gas flow rates are 1.0, 0.4 and 1.2 L min^{-1}, respectively, and the power is 1000 W.

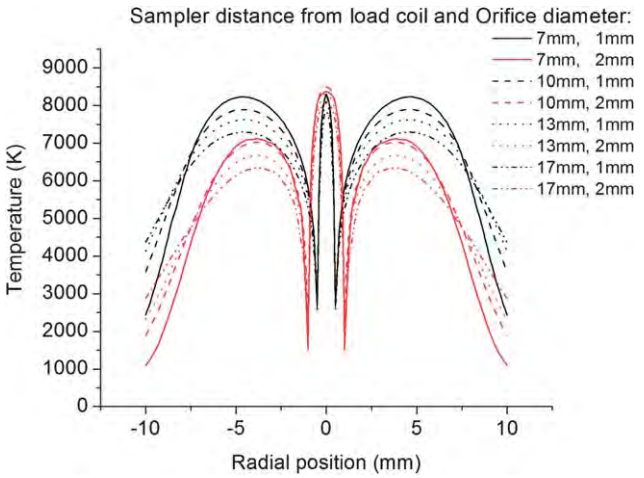

Fig. 3 Radial distributions of the plasma temperature (K) at the place of the sampler for sampler orifice diameters of 1 mm (black lines) and 2 mm (red lines), at a sampler position of 7 mm (solid lines), 10 mm (dashed lines), 13 mm (dotted lines) and 17 mm (dotted-dashed lines) from the load coil.

fixed at 1.5 mm) is larger than the sampler orifice diameter, and in this case, the same results are obtained as in ref. 36. However, in the right column, the diameter of the injector inlet is smaller than the diameter of the sampler orifice, and in this case, the auxiliary gas can pass through the sampler orifice.

Hence it can be concluded that the outgoing flow pattern of the auxiliary gas can be controlled by a combination of the ratios of gas flow rates and the sampler orifice and injector diameters. This can be used to optimize the sampling performance, depending on whether we want only the injector gas to enter the MS, or the injector gas accompanied by some auxiliary gas. The latter can be desired when the auxiliary gas also contains part of the sample ions (or ionic cloud). This is clearly explained by Houk and coworkers in ref. 46. They used a differential mobility analyzer electrostatic classifier to select particles in a specific size range from the laser ablation aerosol to be transported to the plasma. Specifically in Fig. 3 in ref. 46, they compared the size, position and trajectory of both small and large particles in the ICP torch. If an aerosol particle is sufficiently small (typically up to 150 nm), it will be efficiently vaporized and atomized along the central line. Larger particles are less extensively vaporized and atomized in the ICP torch. Also, their ion cloud position in the torch can be on or off the axis. Therefore, depending on the size and the position of the ion cloud of large particles reaching the sampler cone, it is important whether the auxiliary flow can be extracted or not. In ref. 47, Niemax also reported that the ion cloud diameter at the sampler orifice will be different, depending on the spatial position of the atomization. Larger droplets of analyte solution can penetrate deeper into the ICP than smaller droplets before they are desolvated and atomization of the analyte can start.[47] It means that the size of the analyte ion cloud from larger droplets is smaller at the position of the sampler, and probably it is sufficient when only the injector gas passes through the sampler orifice. On the other hand, for smaller droplets, the ion cloud becomes larger at the sampler position, and in this case it will be beneficial when (part of) the auxiliary gas can also be transported into the MS.[47]

Furthermore, it is also clear from Fig. 2 (especially at 13 mm distance from the load coil) that changes in the auxiliary gas path line profiles also affect the plasma temperature profiles close to the sampler (see upper frames). Indeed, the auxiliary gas passes through the region of highest power coupling in the plasma (see red contours in the lower frames), and will therefore be at higher plasma temperature than the injector gas. For an orifice diameter of 2 mm (right column), the auxiliary gas passes through the sampler orifice, and therefore the plasma temperature will be higher near the sampler orifice than in the case of 1 mm orifice diameter (left column), as is clear from Fig. 2. Hence, the gas will pass through the sampler orifice with a higher plasma temperature, which helps to sustain the ions on their way to the detectors. Moreover, with a larger orifice, the cooling effect of the sampler is somewhat lower at the central axis (see also below). This might also have important consequences for the ICP sampling performance, because the gas flow which contains most of the sample ions is less affected by the interface cone.

Fig. 3 shows the plasma temperature as a function of radial position for sample orifice diameters of 1 mm (black lines) and 2 mm (red lines), at a sampler position of 7 mm (solid

lines), 10 mm (dashed lines), 13 mm (dotted lines) and 17 mm (dotted-dashed lines) from the load coil. It is clear that an increase in orifice diameter causes a slightly higher plasma temperature at the center and a clearly lower plasma temperature at the sides, which is explained by the change in the auxiliary gas pathlines, illustrated in Fig. 2 above. Indeed, the hotter auxiliary gas will exit through the sampler cone at 2 mm sampler orifice diameter, yielding a higher plasma temperature at the center, whereas at 1 mm sampler orifice diameter, it will flow out through the sides, resulting in a higher plasma temperature at the sides. Furthermore, an increase in sampler distance from the load coil leads to a lower plasma temperature at the sampler position, because the gas has more time to cool down by emitting radiation after leaving the torch. This drop in the plasma temperature with increasing distance from the load coil was also reported by Hieftje and coworkers.[34]

Fig. 4 illustrates in detail the flow velocity path lines close to the sampler, with an orifice diameter of 1 mm (a) and 1.5 mm (b). Note that the injector gas flow rate is not the same in both figures, *i.e.*, it is equal to 1 L min^{-1} for the 1 mm orifice diameter, and 2.25 L min^{-1} for the 1.5 mm orifice diameter, so that the ratio of the injector gas flow rate to the surface area of the sampler orifice is constant in both cases. It is obvious from Fig. 4 that in both cases the injector gas (colored) can exit through the orifice, as desired, but the interaction between the flow and the metal sampling cone is much more prominent in the case of the smaller orifice diameter (see Fig. 4a), leading to a somewhat lower flow velocity as well as more pronounced cooling of the gas. The latter will result in changes in the composition of the plasma gases that come in contact with the metal surface, *i.e.*, a boundary layer of cooler gases will be formed along the surface of the metal. This effect was also described in the literature. Indeed, Hayhurst *et al.*[48] stated that a larger orifice diameter results in a larger total flow rate into the sampler, which causes a reduction in the boundary layer thickness. This would result in lower oxide levels for larger sampler orifice diameters, which was indeed observed.[41] Moreover, a large sampling orifice was not so easily clogged by concentrated solutions, and because the sampling orifice diameter was significantly larger than the thickness of the boundary layer formed on its edges, the bulk of the plasma flowing into the first vacuum stage had essentially the same composition as the upstream plasma.[44]

Finally, similar to Fig. 2, we can again conclude from Fig. 4b that also in this case, *i.e.*, the diameter of the injector gas inlet equal to the sampler orifice diameter, the auxiliary gas can exit through the sampler, even when the injector gas flow rate is higher than the auxiliary gas flow rate.

(b) Electron number density and gas density

The electron density was calculated by solving the Saha–Eggert equation. Fig. 5 presents the radial electron number density profile at 8 mm from the load coil, for different positions of the sampler, *i.e.* 10 mm (solid line), 13 mm (dashed line) and 17 mm (dotted line) distance from the load coil. The electron density in the central region drops slightly when the sampling position is reduced. Experimentally, Gamez *et al.*[34] and Macedone *et al.*[35] reported the same behavior for the electron temperature and ion density, respectively. The explanation is of course logical, because in the case of the shorter sampling position (10 mm distance from the load coil) the distance between the sampler and the "measurement position" of the electron density, *i.e.*, 8 mm, is only 2 mm, and the cooling of the plasma by the metal sampling cone will be more pronounced, resulting in a lower plasma temperature and hence lower electron density, while in the case of the larger sampling position, the distance between the sampling cone and the "measurement position" is 9 mm, and hence the (cooling) effect of the sampling cone is less pronounced.

In Fig. 6 the radial gas density profile is plotted at the position of the sampler, for the case of 10 mm distance from the load coil, with orifice diameters of 1 mm (black line) and 2 mm (red line). $R = 0$ shows the center of the sampler orifice, or the central axis of the torch. In both cases, two maxima are observed close to the center, which indicate the edges of the sampler orifice, *i.e.* at $R = 0.5$ mm and $R = 1$ mm from the center in the black and red plots, respectively. To explain these density profiles, we refer to the plasma temperature profiles presented

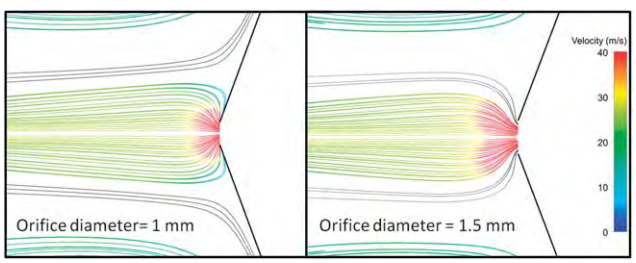

Fig. 4 2D gas flow velocity path lines originating from the injector gas and outer gas inlets, colored by velocity in m s^{-1}, and from the auxiliary gas inlet, colored in black, close to the sampler, which is placed at 10 mm distance from the load coil with an orifice diameter of 1 mm (a) and 1.5 mm (b). The injector gas flow rate is taken as 1 (a) and 2.25 (b) L min^{-1}, to maintain the same ratio of the injector gas flow rate to the surface area of the sampler orifice.

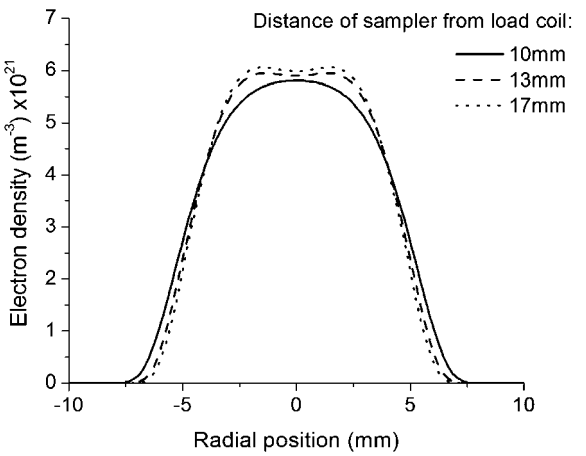

Fig. 5 Radial distributions of the electron number density (m^{-3}) at 8 mm distance from the load coil, for different positions of the sampler, *i.e.* 10 mm (solid line), 13 mm (dashed line) and 17 mm (dotted line) distance from the load coil and a sampler orifice diameter of 1 mm.

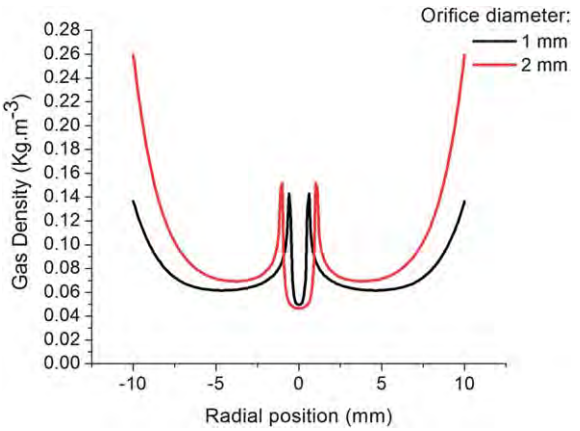

Fig. 6 Radial distributions of the gas density (kg m^{-3}) for sampler orifice diameters of 1 mm (black lines) and 2 mm (red lines), at a sampler position of 10 mm from the load coil.

in Fig. 3. At the center of the orifice, the plasma temperature has its maximum value and two pronounced drops are seen at both sides of it, indicating the edges of the sampler orifice. Indeed, the sampling cone temperature close to the orifice is around 550 K, so it cools down the gas (Fig. 3), and following the ideal gas law, the density rises (Fig. 6). The inverse relationship between plasma temperature and gas density profiles is indeed clear from Fig. 3 and 6. At larger sampler orifice diameter, the cooling effect of the sampling cone at the center will be more moderate, resulting in a somewhat higher plasma temperature and somewhat lower gas density. Hence, the gas will pass through the orifice with a somewhat higher plasma temperature and lower density.

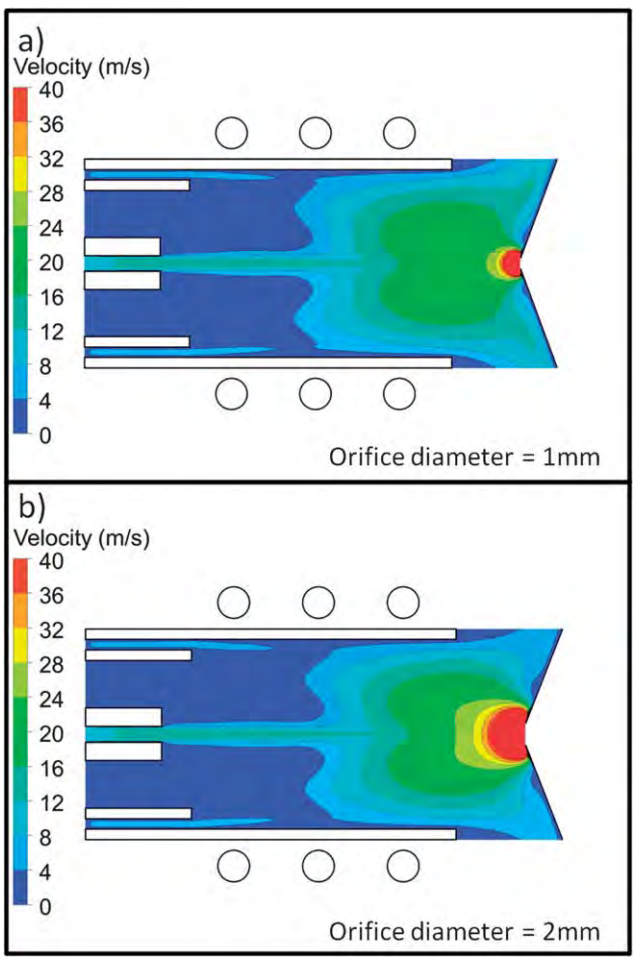

Fig. 7 2D velocity profiles (m s^{-1}) for 1 mm (a) and 2 mm (b) orifice diameters, at the sampler position of 10 mm from the load coil.

(c) Gas velocity

Fig. 7 presents the 2D gas velocity distributions when the sampler cone is placed at 10 mm from the load coil and the orifice diameter is 1 mm (a) and 2 mm (b). A larger sampler orifice results in a larger gas flow velocity in the region close to the sampler. The acceleration of the gas is very prominent in the region close to the sampler and the gas velocity changes strongly with the position in this region. According to our calculation, at the place of the sampler, the plasma ions enter the MS with almost the same velocity in both cases. It means that the maximum value of the gas velocity exiting from the sampler is independent of the sampler orifice size. The value of the Mach number at the center of the orifice, where the flow has its maximum velocity, is around 0.6, and is found to be the same for both orifice sizes. It is mentioned also in ref. 49 that the Mach number and velocity are independent of the size of the orifice. The position of the sampler, also, does not exhibit any considerable effect on the gas velocity.

4 Conclusion

We have computationally investigated the effect of the distance of the sampler cone from the load coil and its orifice diameter on the plasma characteristics in the ICP connected to a MS, in order to obtain a better insight into the effect of these geometrical parameters on the analytical performance of ICP-MS. The fundamental plasma characteristics of the ICP upstream from the sampler, calculated in this work, include the plasma temperature, electron number density, gas density and gas flow velocity.

Our calculations show that by increasing the sampler orifice diameter, the central plasma temperature at the place of the sampler rises slightly and consequently, the gas density reduces a bit, while the gas density is maximum at the edges of the sampler. Furthermore, the gas passes through the sampler orifice with a velocity which is independent of the sampler orifice diameter.

From a zoomed picture of the velocity path lines close to the sampler, it is clear that the interaction of gas with the interface cone reduces by increasing the sampler orifice diameter, which causes a lower plasma temperature reduction at the place of the sampler cone and leads to more efficient gas transfer to the mass spectrometer.

Furthermore, our calculation results have demonstrated that the sampler orifice diameter should be equal to or larger than the injector inlet diameter to make sure that the auxiliary gas

can also pass through the sampler orifice, which is desired when the ion cloud is large at the place of the sampler. On the other hand, to ensure that only the injector gas can enter the mass spectrometer, which is necessary to optimize the detection efficiency of the sample in the case when the ion cloud diameter is small, *i.e.*, when the analyte ions are transported only by the injector gas, the sampler orifice diameter should be smaller than the injector inlet diameter.

Finally, the plasma temperature at the place of the sampler decreases slightly with the increasing distance of the sampler from the load coil, and at a fixed measurement position upstream from the sampler, the electron density drops when the sampling position is reduced.

Acknowledgements

The authors gratefully acknowledge financial support from the University of Antwerp through the Methusalem Financing. This work was carried out using the Turing HPC infrastructure at the CalcUA core facility of the Universiteit Antwerpen, a division of the Flemish Supercomputer Center VSC, funded by the Hercules Foundation, the Flemish Government (department EWI) and the Universiteit Antwerpen.

References

1 R. S. Houk, V. A. Fassel and H. J. Svec, *Inductively Coupled Plasma – Mass Spectrometry: Sample Introduction, Ionization, Ion Extraction, and Analytical Results in Dynamic Mass Spectrometry*, ed. D. Price and J. F. J. Todd, Heyden, London, 6 (1981) pp. 234–251.

2 I. I. Stewart, C. E. Hensman and J. W. Olesik, Influence of gas sampling on analyte transport within the ICP and ion sampling for ICP-MS studied using individual, isolated sample droplets, *Appl. Spectrosc.*, 2000, **54**, 164–174.

3 G. Meyer, R. Foster, A. Van der Hoeff, T. Albert, S. Luan, K. Hu, S. Karpova-Nadel and J. Schmeizel, Increasing laboratory productivity by combining ICP optical emission with ICP mass spectrometry, *Am. Lab.*, 1996, **28**, 21–24.

4 H. P. Longerich, Mass spectrometric determination of the temperature of an argon inductively coupled plasma from the formation of the singly charged monoxide rare earths and their known dissociation energies, *J. Anal. At. Spectrom.*, 1989, **4**, 491–497.

5 K. Lepla, M. A. Vaughan and G. Horlick, Simultaneous atomic emission and mass spectrometric measurements on an inductively coupled plasma, *Spectrochim. Acta, Part B*, 1991, **46**, 967–973.

6 R. S. Houk and Y. Zhai, Comparison of mass spectrometric and optical measurements of temperature and electron density in the inductively coupled plasma during mass spectrometric sampling, *Spectrochim. Acta, Part B*, 2001, **56**, 1055–1067.

7 R. S. Houk, J. K. Schoer and J. S. Crain, Deduction of excitation temperatures for various analyte species in inductively coupled plasmas from vertically-resolved emission profiles, *Spectrochim. Acta, Part B*, 1987, **42**, 841–852.

8 L. Pei-Qi, G. Pei-Zhing, L. Tei-Zheng and R. S. Houk, Langmuir probe measurements of electron temperature in an ICP, *Spectrochim. Acta, Part B*, 1988, **43**, 273–285.

9 H. Niu and R. S. Houk, Fundamental aspects of ion extraction in inductively coupled plasma mass spectrometry, *Spectrochim. Acta, Part B*, 1996, **51**, 779–815.

10 J. S. Crain, F. G. Smith and R. S. Houk, Mass spectrometric measurement of ionization temperature in an inductively coupled plasma, *Spectrochim. Acta, Part B*, 1990, **45**, 249–259.

11 B. S. Duersch, Y. Chen, A. Ciocan and P. B. Farnsworth, Optical measurements of ion density in the second vacuum stage of an inductively coupled plasma mass spectrometer, *Spectrochim. Acta, Part B*, 1998, **53**, 569–579.

12 B. S. Duersch and P. B. Farnsworth, Characterization of the ion beam inside the skimmer cone of an inductively coupled plasma mass spectrometer by laser excited atomic and ionic fluorescence, *Spectrochim. Acta, Part B*, 1999, **54**, 545–555.

13 D. M. Chambers and G. M. Hieftje, Fundamental studies of the sampling process in an inductively coupled plasma mass spectrometer. II. Ion kinetic energy measurements, *Spectrochim. Acta, Part B*, 1991, **46**, 761–784.

14 A. L. Gray, R. S. Houk and J. G. Williams, Langmuir probe potential measurements in the plasma and their correlation with mass spectral characteristics in inductively coupled plasma mass spectrometry, *J. Anal. At. Spectrom.*, 1987, **2**, 13–20.

15 R. S. Houk, J. K. Schoer and J. S. Crain, Plasma potential measurements for inductively coupled plasma mass spectrometry with a center-tapped load coil, *J. Anal. At. Spectrom.*, 1987, **2**, 283–286.

16 R. S. Houk, B. R. LaFreniere, H. B. Lim and V. A. Fassel, Extraction Discharge Source for Enhancing Analyte Line Intensities in Inductively Coupled Plasma Atomic Emission Spectrometry, *Appl. Spectrosc.*, 1987, **41**, 391–395.

17 R. K. Winge, J. S. Crain and R. S. Houk, A High Speed Photographic Study of Plasma Fluctuations and Undissociated Particles in ICP-MS, *J. Anal. At. Spectrom.*, 1991, **6**, 601–604.

18 H. Ma, N. Taylor and P. B. Farnsworth, The effect of the sampling interface on spatial distributions of barium ions and atoms in an inductively coupled plasma ion source, *Spectrochim. Acta, Part B*, 2009, **64**, 384–391.

19 S. A. Lehn, K. A. Warner, M. Huang and G. M. Hieftje, Effect of an inductively coupled plasma mass spectrometry sampler interface on electron temperature, electron number density, gas-kinetictemperature and analyte emission intensity upstream in the plasma, *Spectrochim. Acta, Part B*, 2002, **57**, 1739–1751.

20 D. J. Douglas and J. B. French, Gas dynamics of the inductively coupled plasma mass spectrometry interface, *J. Anal. At. Spectrom.*, 1988, **3**, 743–747.

21 R. L. Spencer, J. Krogel, J. Palmer, A. Payne, A. Sampson, W. Somers and C. N. Woods, Modeling the gas flow upstream and in the sampling nozzle of the inductively coupled plasma mass spectrometer *via* the Direct Simulation Monte Carlo algorithm, *Spectrochim. Acta, Part B*, 2009, **64**, 215–221.

22 R. L. Spencer, N. Taylor and P. B. Farnsworth, Comparison of calculated and experimental flow velocities from the sampling cone of an inductively coupled plasma mass spectrometer, *Spectrochim. Acta, Part B*, 2009, **64**, 921–924.
23 H. Lindner and A. Bogaerts, Multi-element model for the simulation of inductively coupled plasmas: effects of helium addition to the central gas stream, *Spectrochim. Acta, Part B*, 2011, **66**, 421–431.
24 H. Lindner, A. Murtazin, S. Groh, K. Niemax and A. Bogaerts, Simulation and experimental studies on plasma temperature, flow velocity and injector diameter effects for an inductively coupled plasma, *Anal. Chem.*, 2011, **83**, 9260–9266.
25 M. Aghaei, H. Lindner and A. Bogaerts, Effect of a mass spectrometer interface on inductively coupled plasma characteristics: a computational study, *J. Anal. At. Spectrom.*, 2012, **27**, 604–610.
26 J. H. Macedone, D. J. Gammon and P. B. Farnsworth, Factors affecting analyte transport through the sampling orifice of an inductively coupled plasma mass spectrometer, *Spectrochim. Acta, Part B*, 2001, **56**, 1687–1695.
27 S. Kaneco, T. Nomizo, T. Tanaka, N. Mizutani and H. Kawaguchi, Optimization of operating conditions in individual airborne particle analysis by inductively coupled plasma mass spectrometry, *Anal. Sci.*, 1995, **11**, 835–840.
28 W. G. Diegor and H. P. Longerich, Parameter interaction in signal optimization of an ICP mass spectrometer, *At. Spectrosc.*, 2000, **21**, 111–117.
29 H. P. Longerich, B. J. Fryer, D. F. Strong and C. J. Kantipuly, Effects of operating conditions on the determination of the rare earth elements by inductively coupled plasma-mass spectrometry (ICP-MS), *Spectrochim. Acta, Part B*, 1987, **42**, 75–92.
30 S. E. Long and R. M. Browner, Optimization in inductively coupled plasma mass spectrometry, *Analyst*, 1986, **111**, 901–906.
31 Q. Xie and R. Kerrich, Optimization of operating conditions for improved precision of zirconium and hafnium isotope ratio measurement by inductively coupled plasma mass spectrometry (ICP-MS), *J. Anal. At. Spectrom.*, 1995, **10**, 99–103.
32 B. T. G. Ting and M. Janghorbani, Optimization of instrumental parameters for the precise measurement of isotope ratios with inductively coupled plasma mass spectrometry, *J. Anal. At. Spectrom.*, 1988, **3**, 325–336.
33 G. Gamez, S. A. Lehn, M. Huang and G. M. Hieftje, Effect of Mass Spectrometric sampling interface on the fundamental parameters of an inductively coupled plasma as a function of its operating conditions. Part I. Applied RF power and vacuum, *Spectrochim. Acta, Part B*, 2007, **62**, 357–369.
34 G. Gamez, S. A. Lehn, M. Huang and G. M. Hieftje, Effect of Mass Spectrometric sampling interface on the fundamental parameters of an inductively coupled plasma as a function of its operating conditions. Part II. Central-gas flow rate and sampling depth, *Spectrochim. Acta, Part B*, 2007, **62**, 370–377.
35 J. H. Macedone, A. A. Mills and P. B. Farnsworth, Optical measurements of ion trajectories through the vacuum interface of an inductively coupled plasma mass spectrometer, *Appl. Spectrosc.*, 2004, **58**, 463–467.
36 M. Aghaei, H. Lindner and A. Bogaerts, Optimization of operating parameters for inductively coupled plasma mass spectrometry: a computational study, *Spectrochim. Acta, Part B*, 2012, **76**, 56–64.
37 A. L. Gray and A. R. Date, Inductively coupled plasma source mass spectrometry using continuum flow ion extraction, *Analyst*, 1983, **108**, 1033–1050.
38 G. M. Hieftje and G. H. Vickers, Developmentsin plasma source/mass spectrometry, *Anal. Chim. Acta*, 1989, **216**, 1–24.
39 F. E. Lichte, A. L. Meier and J. G. Crock, Determination of the rare-earth elements in geological materials by inductively coupled plasma mass spectrometry, *Anal. Chem.*, 1987, **59**, 1150–1157.
40 J. S. Crain, R. S. Houk and F. G. Smith, Matrix interferences in inductively coupled plasma-mass spectrometry: some effects of skimmer orifice diameter and ion lens voltages, *Spectrochim. Acta, Part B*, 1988, **43**, 1355–1364.
41 M. A. Vaughan and G. Horlick, Effect of sampler and skimmer orifice size on analyte and analyte oxide signals in inductively coupled plasma mass spectrometry, *Spectrochim. Acta, Part B*, 1990, **45**, 1289–1299.
42 H. P. Longerich, B. J. Fryer, D. F. Strong and C. J. Kanttpuly, Effects of operating conditions on the determination of the rare earth elements by inductively coupled plasma-mass spectrometry (ICP-MS), *Spectrochim. Acta, Part B*, 1987, **42**, 75–92.
43 D. Günter, H. P. Longerich, S. E. Jackson and L. Forsythe, Effect of sampler orifice diameter on dry plasma inductively coupled plasma mass spectrometry (ICP-MS) backgrounds, sensitivities, and limits of detection using laser ablation sample introduction, *Fresenius' J. Anal. Chem.*, 1996, **355**, 771–773.
44 N. Taylor and P. B. Farnsworth, Experimental characterization of the effect of skimmer cone design on shock formation and ion transmission efficiency in the vacuum interface of an inductively coupled plasma mass spectrometer, *Spectrochim. Acta, Part B*, 2012, **69**, 2–8.
45 ANSYS FLUENT 12.0/12.1 Documentation, 2009.
46 D. C. Perdian, S. J. Bajic, D. P. Baldwin and R. S. Houk, Time-resolved Studies of Particle Effects in Laser Ablation ICP-MS Part I. Investigation of Nanosecond and Femtosecond Pulse Width Lasers and Devices for Particle Size Selection, *J. Anal. At. Spectrom.*, 2008, **23**, 325–335.
47 K. Niemax, Considerations about the detection efficiency in inductively coupled plasma mass spectrometry, *Spectrochim. Acta, Part B*, 2012, **76**, 65–69.
48 A. N. Hayhurst, D. B. Kittelson and N. R. Telford, Mass spectrometric sampling of ions from atmospheric pressure flames – II: aerodynamic disturbance of a flame by the sampling system, *Combust. Flame*, 1977, **28**, 123–135.
49 A. N. Hayhurst, Mass Spectrometric Sampling of a Flame, *Combust., Explos. Shock Waves (Engl. Transl.)*, 2012, **48**, 516–525.

